Proton-induced fission cross sections on ^{208}Pb at high kinetic energies

J. L. Rodríguez-Sánchez,[1] J. Benlliure,[1,*] J. Taïeb,[2] A. Chatillon,[2] C. Paradela,[1] Y. Ayyad,[1,†] G. Bélier,[2] G. Boutoux,[2,‡] E. Casarejos,[3] T. Gorbinet,[2] B. Laurent,[2] J.-F. Martin,[2] E. Pellereau,[2] H. Álvarez-Pol,[1] L. Audouin,[4] D. Cortina-Gil,[1] A. Heinz,[5] A. Kelić-Heil,[6] B. Pietras,[1] D. Ramos,[1] C. Rodríguez-Tajes,[7] D. Rossi,[6] H. Simon,[6] L. Tassan-Got,[4] J. Vargas,[1] and B. Voss[6]

[1]*Universidad de Santiago de Compostela, E-15782 Santiago de Compostela, Spain*

[2]*CEA, DAM, F-91297 Arpajon, France*

[3]*Universidad de Vigo, E-36200 Vigo, Spain*

[4]*Institut de Physique Nucléaire d'Orsay, F-91406 Orsay, France*

[5]*Chalmers University of Technology, SE-412 96 Gothenburg, Sweden*

[6]*GSI Helmholtzzentrum für Schwerionenforschung GmbH, D-64291 Darmstadt, Germany*

[7]*Grand Accélérateur National d'Ions Lourds, F-14076 Caen, France*

(Received 12 October 2014; published 5 December 2014)

Total fission cross sections of ^{208}Pb induced by protons have been determined at 370A, 500A, and 650A MeV. The experiment was performed at GSI Darmstadt where the combined use of the inverse kinematics technique with an efficient detection setup allowed us to determine these cross sections with an uncertainty below 6%. This result was achieved by an accurate beam selection and registration of both fission fragments in coincidence which were also clearly distinguished from other reaction channels. These data solve existing discrepancies between previous measurements, providing new values for the Prokofiev systematics. The data also allow us to investigate the fission process at high excitation energies and small deformations. In particular, some fundamental questions about fission dynamics have been addressed, which are related to dissipative and transient time effects.

DOI: 10.1103/PhysRevC.90.064606 PACS number(s): 24.75.+i, 25.40.Sc, 25.85.Ge

I. INTRODUCTION

Proton-induced reactions on lead are of importance for the understanding the fission process at high energies, but also because of their impact in spallation neutron sources.

Following its discovery 76 years ago, a complete microscopic description of the fission process is not yet available. Significant progress was achieved in the last years by new microscopic descriptions of the nuclear potential governing the fission process [1,2], detailed measurements of fission cross sections [3–6], and the characteristics of the final fission fragments [7–10].

Despite this progress, a satisfactory understanding of the fission probabilities for low-fissility systems has not been reached. For those systems fission only appears at excitation energies well above the fission barrier, where a strong competition with other deexcitation channels such as nucleon or cluster evaporation sets in [11]. Under such conditions it was shown that descriptions of the fission process based on the transition-state approach [12] are unsatisfactory. These models underpredict pre-scission gamma and nucleon emission [13–15] and overpredict fission probabilities [16–18].

Models describing fission as a diffusion process across the barrier governed not only by the nuclear potential and phase space, but also by the coupling between intrinsic and collective degrees of freedom described by a dissipation parameter [19], seem to provide a better description of fission. In this context the initial conditions of the fissioning system play a decisive role [20–24]. Proton-induced fission on lead at relativistic energies fulfills the conditions established for the optimal manifestation of dissipative and transient effects in fission [3,6]. In this case, the small shape distortion expected in proton-induced reactions on a spherical nucleus such as lead, the high excitation energies and the low angular momentum gained, provide well-defined initial conditions for fissioning nuclei [21,22,25,26].

Moreover, a lead-bismuth eutectic is proposed as an optimum target material for spallation-neutron sources irradiated with relativistic protons [27–32]. The neutron excess of this material enhances the number of emitted neutrons per incident proton. In addition, the use of a liquid eutectic solves the problem of target damages due to the high irradiation dose. Nevertheless, radiological effects induced by activation create concern for the use of these targets [33,34]. Therefore, a complete inventory of the residual nuclei produced in these reactions is required [35]. In particular the production of gaseous fission residues such as krypton or xenon may have an important radiological impact.

The complete inventory of residual fragments produced in spallation reactions induced by protons on lead at 500A and 1000A MeV has been already determined [36,37]. These measurements were performed in inverse kinematics by employing a high-resolving-power magnetic spectrometer. Despite the accuracy of the spectrometer, which was sufficient to identify the reaction products in terms of their mass and atomic number, the measurement of fission residues was affected by the limited angular and momentum acceptance of the spectrometer [38]. This could explain the unexpected high

*Corresponding author: j.benlliure@usc.es

†Present address: Research Center for Nuclear Physics, Osaka University, Ibaraki, Osaka 567-0047, Japan.

‡Present address: Université Bordeaux, F-33405 Talence, France.

fission cross section obtained at 500A MeV (232 mb) [36]. Indeed, a later measurement of this cross section based also on the inverse kinematics technique, but detecting both fission fragments in coincidence, provided a lower fission cross section (146 mb) [39].

Proton-induced fission cross sections on lead have also been measured in direct kinematic experiments covering a large range in energy [40]. In this case limitations associated with the absorption of the fragments in the target and the techniques used for the identification of the fission channel could also explain the discrepancies, up to 50%, observed in these measurements. Therefore, the systematic of the proton on lead fission cross section established by Prokofiev some time ago [40] could be questioned.

In this work we present a new accurate measurement of the fission cross section in reactions induced by protons on lead at 370A, 500A, and 650 A MeV. The experiment was also performed in inverse kinematics and takes advantage of a next-generation experimental setup [41–44]. This setup provides coincident measurement of both fission fragments, as well as their identification in atomic number. Moreover, high-precision tracking of the trajectories of the two fragments made it possible to separate fission reactions produced in the hydrogen target from reactions induced in other layers of matter traversed by the beam. These measurements allow us to clarify the discrepancies between the existing measurements, establish a new systematic, and contribute to the understanding of the fission process at high excitation energies.

II. EXPERIMENT

The most important feature of this experiment is the use of the inverse-kinematics method where a light target, in this case hydrogen, is bombarded with heavy relativistic projectiles: ^{208}Pb ions. This experimental approach has several advantages with respect to conventional experiments performed in direct kinematics. The fission fragments leave the target with high energy, covering a narrow angular range (less than 50 mrad) in the forward direction. These features facilitate the detection and identification of both fission fragments. In order to achieve these conditions, the experiment was performed at GSI Darmstadt where the SIS18 synchrotron is able to accelerate beams of ^{208}Pb ions to 370A, 500A, and 650A MeV with a current of the order of 10^5 ions/s.

The accurate determination of the fission cross sections requires a precise measurement of the number of incoming projectiles and an unambiguous identification and counting of the fission events. To register and identify both fission fragments, an advanced detection setup was mounted behind the target providing a coincident measurement of the two fragments and covering the complete angular range in the forward direction. This setup permitted us to separate fission from other reaction channels, to identify the atomic number of both fission fragments and to reconstruct their trajectories in order to determine the reaction vertex. All these features are crucial for obtaining the setup detection efficiency and, therefore, the total fission cross section with high accuracy.

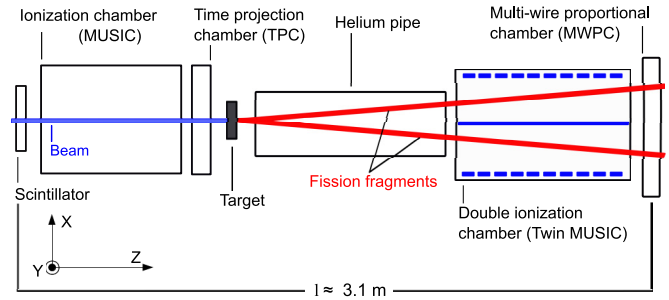

FIG. 1. (Color online) Top schematic view of the experimental setup used in this experiment. Sizes are not to scale.

A. Description of the experimental setup

Figure 1 shows a schematic representation of the detector setup used in this experiment. This setup can be separated into two parts: one to characterize the beam and another to identify and count the fission events. The first part consists of a plastic scintillator detector ($50 \times 32 \times 1.5$ mm^3) [45], an ionization chamber (MUSIC) [46], and a time projection chamber (TPC) [47] that provide the identification in atomic number of the beam ions and their transverse position, respectively.

Measurements were performed with a cylindrical target (11.24 mm long and 30 mm diameter) filled with liquid-hydrogen of (85.9 ± 1.5) mg/cm^2 produced in a cryostat [48]. The target was isolated by two windows consisting of aluminized-mylar foils with a thickness of 35 μm.

The second part of the setup consists of a double ionization chamber (Twin MUSIC) [49] and a multiwire proportional counter (MWPC). Twin MUSIC has a central vertical cathode that divides its volume into two active parts; both are 60 cm long, 20 cm high and 10 cm wide. The atomic number of each fragment is deduced from the energy signals registered in each side by the ten anodes parallel to the common cathode. These ten anodes also provide drift-time measurements which allow us to obtain the polar angles of both fission fragments with a resolution of 0.5 mrad full width at half maximum (FWHM). Finally, a MWPC, similar to those designed for the ALICE experiment [50], provides horizontal (X) and vertical (Y) positions of the fission fragments with a resolution of 200 μm and 1 mm (FWHM), respectively. In addition, an aluminium pipe filled with helium gas was mounted between the target and the double ionization chamber to reduce the energy and angular straggling of the fission fragments.

B. Selection of primary beam and fission events

For extracting fission cross sections, one needs to determine the number of projectiles impinging on the target. An identification of the projectiles is needed to exclude contaminants. For this purpose, the ionization chamber MUSIC, placed in front of the target, is used to register the projectiles event by event, while recording also their energy loss. This additional information is needed because the incoming ^{208}Pb projectiles may react also in the different layers of matter placed upstream from the liquid-hydrogen target, in particular the plastic scintillator. For those events the lead ions may lose protons or neutrons, thus resulting in a cocktail beam reaching the target.

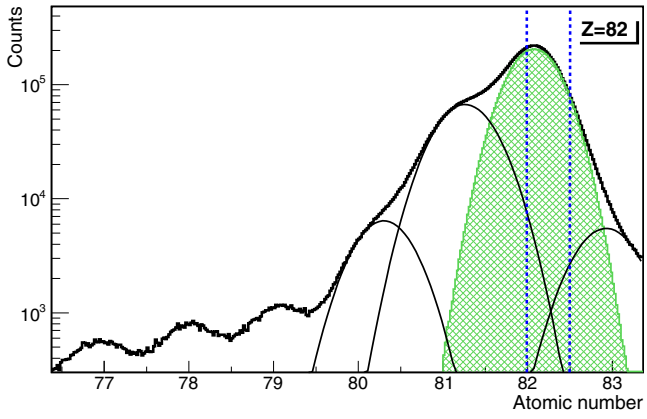

FIG. 2. (Color online) Atomic-number histogram of the ions detected with the ionization chamber placed before the target for the reaction ^{208}Pb(500AMeV) + p.

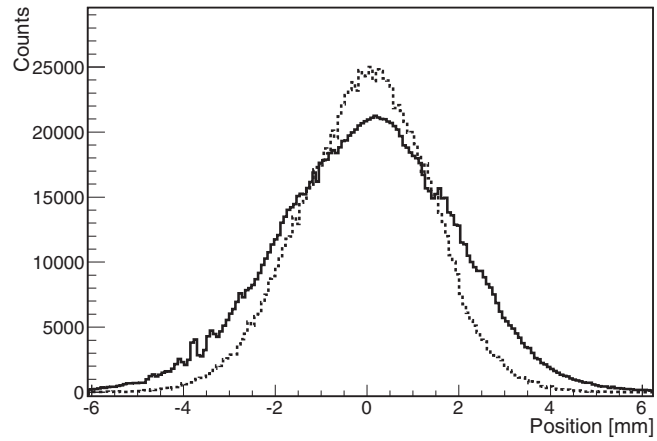

FIG. 3. Position distributions of the beam ions in horizontal (solid histogram) and vertical direction (dotted histogram) as determined by the TPC for our measurement at 500A MeV.

Projectiles with atomic numbers different from $Z = 82$ could be identified based on their energy-loss signal measured in the MUSIC chamber in front of the target. Unfortunately, reaction channels in which only neutrons are removed could not be disentangled. However, their nuclear reaction probability in the matter placed before the target is evaluated to be less than 0.5% of the total events, rendering their contribution negligible.

Figure 2 shows the atomic-number histogram deduced from the energy-loss signals registered by the MUSIC chamber. Only the ions with an atomic number inside the window defined by the two vertical lines in Fig. 2 are considered as ^{208}Pb projectiles. By fitting the different peaks in the histogram to Gaussian functions one can determine the contribution of each nuclear charge.

As can be seen in the figure, the window contains three nuclear charges leaving the contamination of ions with $Z \neq 82$ to be less than 1.6%, 1.1% for $Z = 81$ and 0.5% for $Z = 83$. $Z = 81$ projectiles are produced in knock-out reactions upstream from the target while $Z = 83$ is attributable to nuclear charge-exchange reactions. Moreover, a TPC chamber, calibrated with a mask, is used to check the impinging position of the projectile ions at the target. Both position distributions are shown in Fig. 3. The widths of both distributions are less than 4.5 mm (FWHM). Similar distributions are obtained for the three beam energies used in this work.

Fission fragments can be identified by atomic number using the Twin MUSIC ionization chamber. This detector provides the identification by measuring the energy-loss signals registered by the ten anodes parallel to the common cathode. These anodes provide also the angle and the position of both fission fragments due to their drift time measurements, in the two gas volumes, right and left of the common cathode. Figure 4 shows the two-dimensional spectrum of the energy lost by the fragments (in channels) registered in the two parts of the Twin MUSIC chamber. This spectrum is collected under the condition defined by the window in Fig. 2. Fission events are selected by the triangular window indicated in Fig. 4. Fragmentation reaction residues and direct-beam ions populate the edges of the spectrum. We can also observe beam pileup that is registered in both sides of the chamber and populates the upper right corner of the figure. As can be seen in the figure, fission fragments are well separated from other reaction channels.

However, fission events can also be induced in other layers of matter traversed by the beam. Luckily, the contribution to fission of each layer of matter can be tracked back by using the Twin MUSIC, which provides the angle on the plane X-Z and the horizontal position of both fission fragments. The reconstruction is made taking into account that fission fragments follow straight trajectories inside the Twin MUSIC. These trajectories are obtained from linear fits of the drift-time signals registered by the ten anodes. The position where fission took place is defined as the intersection point, reaction vertex, between the left and right trajectories. The reconstruction of fission reaction vertex is shown in Fig. 5. This spectrum is collected under the conditions defined by the window in Fig. 2 and the triangular window in Fig. 4. It is clear from the figure

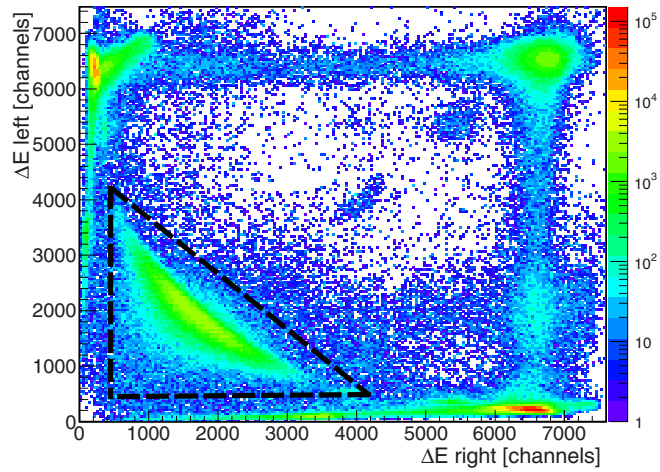

FIG. 4. (Color online) Scatter plot of the energy-loss signals registered by the two gas volumes of the Twin MUSIC chamber for the reaction ^{208}Pb(500AMeV) + p. Fission fragments are located inside the triangular window.

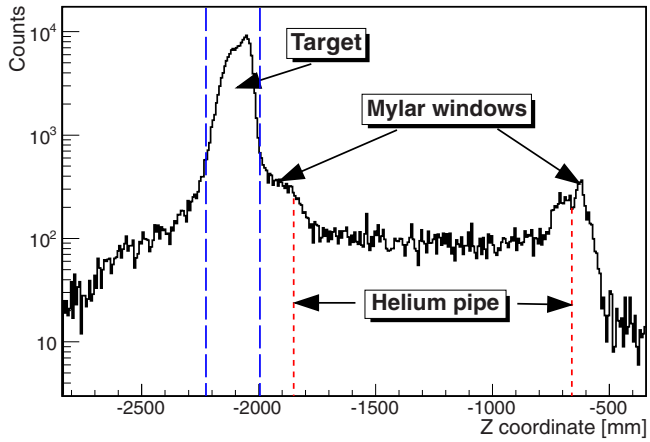

FIG. 5. (Color online) Reconstruction of the fission reaction vertex along the Z coordinate using the tracking capabilities, taking the position of the multiwire proportional chamber as reference point. The long-dashed lines define the window of fission events taking place inside the hydrogen volume for the reaction ^{208}Pb(500AMeV) + p.

that the Twin MUSIC tracking makes it possible to separate between the fission events produced at the target position and fissions originating from other layers of matter, such as the helium gas inside of the pipe or the air between the windows of the target and the helium pipe. However, we cannot separate the contribution from the aluminized-mylar windows because these windows have a thickness of 35 μm and their reaction probabilities are negligible. Only events inside the window, defined by the two long-dashed lines in Fig. 5, are counted as fission.

In Fig. 6 we present a cluster plot of the energy-loss signals registered by the two sections of the Twin MUSIC taking the conditions indicated in Figs. 2, 4, and 5 into account. In this figure, we can see a clear identification of fission events.

However, as will be shown in Sec. II C, the detection probability of the experimental setup does not fully reach 100% and thus not all fission events are contained inside the window of Fig. 5, but this can be easily corrected.

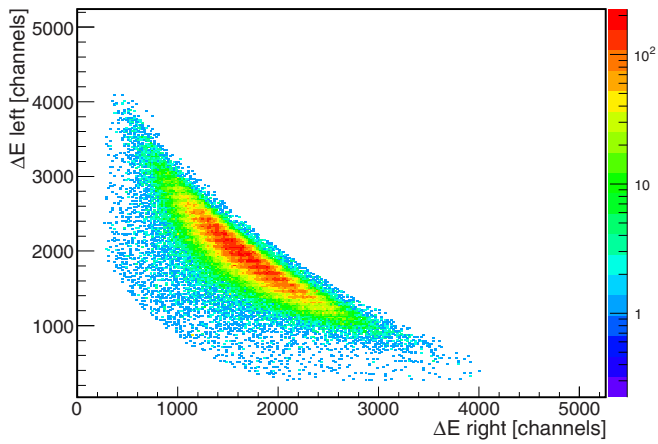

FIG. 6. (Color online) Energy loss of the two fission fragments measured independently in the two parts of the Twin MUSIC plotted versus each other under the conditions shown in Figs. 2, 4, and 5.

C. Detection efficiency of fission events

An important factor to obtain an accurate value of the cross sections is to determine the efficiency of the experimental setup. The main contributions to the detection efficiency are the finite transversal size of the primary beam and its alignment with respect to the cathode placed in the middle of the Twin MUSIC chamber. Fission fragments emitted close to the vertical plane may hit the cathode or pass through the same part of the Twin MUSIC chamber without being registered as fission events. Moreover, fission fragments with a very large angular aperture could hit the aluminium pipe placed in front of the Twin MUSIC chamber reducing thereby the fission detection efficiency. To evaluate the losses on the cathode of the Twin MUSIC we use the MWPC chamber, which allows us to evaluate the shadow induced by the cathode plane. Figure 7 shows the horizontal position of the fission fragments recorded by the MWPC chamber. This spectrum is collected under the condition defined by the window in Fig. 5, i.e., fission events induced by the hydrogen target. In the figure, the shadow due to the cathode is indicated with two vertical lines. The full line shows the result of fitting the distribution with a function defined as the sum of a fourth-order polynomial and a Gaussian. The loss of fission events is estimated based on the difference between the fit and the measured spectrum, obtaining a value around 4.5% for the reaction ^{208}Pb(500AMeV) + p.

Fission events lost because both fragments passed through the same part of the Twin MUSIC chamber are estimated by using a simulation. In this simulation, based on the GEANT4 code [51,52], fission events were generated with the reaction models INCL4.6 [53] and ABLA07 [54] and then propagated through the experimental setup taking electromagnetic and

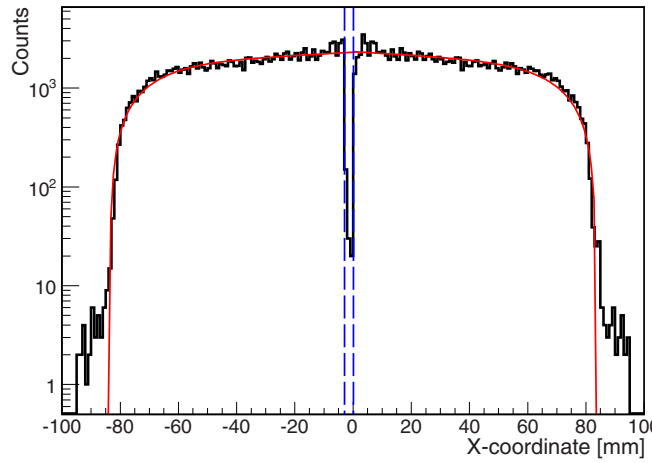

FIG. 7. (Color online) Horizontal (x coordinate) position of the fission fragments recorded by the MWPC chamber for the reaction ^{208}Pb(500AMeV) + p. The two dashed vertical lines indicate the shadow due to the cathode in the center of the Twin MUSIC chamber. The full line is the result of a fit to the histogram.

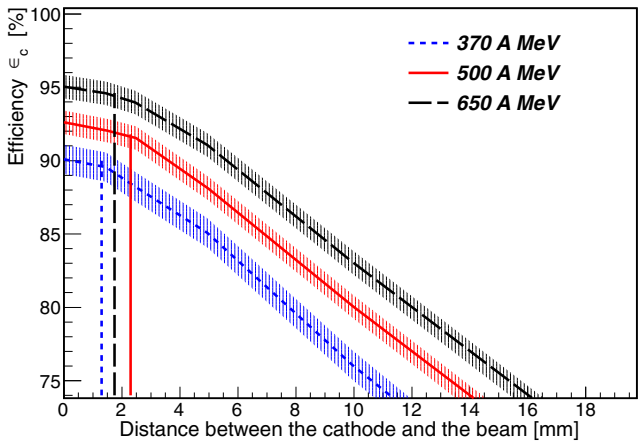

FIG. 8. (Color online) Simulated efficiency for the detection of both fission fragments in the same section of the Twin MUSIC detector as a function of the misalignment distance between the beam and the central cathode of the detector for the three energies investigated in this work. The vertical lines represent the mean value of the measured misalignment for each energy.

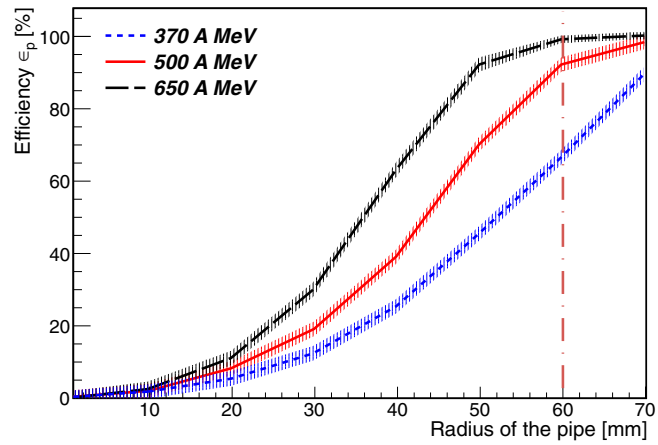

FIG. 9. (Color online) Simulated geometrical efficiency due to the finite size of the helium pipe located between the target and the Twin MUSIC detector. The vertical line represents the pipe radius.

nuclear interactions in all layers of matter into account. Fission fragments originating from fissions in the target were simulated based on the target thickness (11.24 mm) and the beam profile (4 mm FWHM).

This simulation provides the probability that both fission fragments pass through the same part of the Twin MUSIC chamber, which depends on the misalignment between the cathode and the horizontal position of the beam ions. The results of the simulation are shown in Fig. 8. This figure represents the average efficiency (lines) with its associated uncertainty (dashed area) as a function of the distance between the beam and the cathode of the Twin MUSIC for the three energies used in the experiment. The vertical lines represent the mean position of the beam ions for each energy obtained with the MWPC detector placed behind the Twin MUSIC. One can see that, as expected, the efficiency decreases with misalignment between the beam ions and the cathode of the Twin MUSIC detector and increases with energy of the beam.

The simulation is also used to obtain the efficiency loss due to the limited size of the aluminium pipe placed in front of the Twin MUSIC chamber. In this case, the efficiency depends on the radius of the pipe and the energy of the beam. The results of the simulation are shown in Fig. 9 with their associated uncertainty.

III. RESULTS

The total cross section for proton-induced fission of ^{208}Pb was measured at three energies. The number of projectiles (N_p) is determined based on the condition shown in Fig. 2. The number of fission events (N_f) is obtained from the condition indicated in Fig. 5. Their statistical uncertainties are given by Poisson statistics according to the observed number of counts, and for the three measurements they were below 1%. The final results for the measured fission yields ($n_f = N_f/N_p$), corrections and fission cross sections are listed in Table I.

As can be seen in Table I, all applied corrections are rather small, the largest being those corresponding to the attenuation of the beam intensity in the target, the lost fission events in the helium pipe, and the detection efficiency of the Twin MUSIC chamber. The correction of the beam attenuation in the target is obtained from the reaction probability of the incoming projectiles in half of the target thickness calculated with the codes INCL4.6 [53] and ABLA07 [54]. The obtained corrections for the three energies, 370A, 500A, and 650A MeV, are 3.6%, 3.8%, and 4.0%, respectively. Secondary reactions of the beam ions in the target are also evaluated based on the nuclear reaction rate in half of the target thickness. The obtained corrections are below 2.2% for all energies. Moreover, the fission fragments could also undergo secondary reactions between the target and the Twin MUSIC chamber and not be counted as fission events. The corresponding probability for the different layers of matter is below 0.4% for the three experimental energies. The systematic uncertainties associated with these corrections are also listed in Table I.

The results obtained for the total fission cross section are displayed in Fig. 10 (full circles) as a function of the kinetic energy of the proton and compared to previous measurements reported in the literature for the reactions $p + {}^{\text{nat}}$Pb and ^{208}Pb $+ p$. Fission cross sections of $^{\text{nat}}$Pb(p, f) are expected to be above the ones of ^{208}Pb(p, f) because of the lower fission barriers of the naturally abundant lead, with more proton-rich isotopes. The expected difference between the fission cross sections of ^{208}Pb(p, f) and $^{\text{nat}}$Pb(p, f) is less than 10% (see Sec. IV).

As can be seen in the figure, our data have, in general, better accuracy than any of the previous data. Moreover, our measurement at 500 MeV is in perfect agreement with the recent measurement of Schmidt and collaborators (full triangle up) [39] using a similar detection setup. However, the cross section obtained by Fernández and collaborators (full square) [36] using the magnetic spectrometer FRS at GSI exhibits an important deviation with respect to our results and the general systematics. This deviation could be due to the limited acceptance of the spectrometer used in that work [38].

TABLE I. Beam energy, fission yields ($n_f = N_f/N_p$), corrections for Twin MUSIC efficiencies, fission events lost on the helium pipe, beam attenuation in the target, secondary reactions of the beam, and fission background from the reconstruction of Fig. 5. The total fission yield n_f^{tot} represents the corrected fission yield, $n_f^{tot} = [n_f(1 - f_{sr})(1 - f_{br})]/[\varepsilon_{TwinMUSIC}\varepsilon_p(1 - f_{beam})]$. The fission cross section is given by $\sigma = -\ln(1 - n_f^{tot})/N_t$, where N_t represents the number of nuclei in the target per unit area.

Energy [MeV]	Fission yield n_f	Twin MUSIC efficiency $\varepsilon_{TwinMUSIC}$ [%]	Pipe correction ε_p [%]	Beam attenuation f_{beam} [%]	Secondary reactions f_{sr} [%]	Background reconstruction f_{br} [%]	Total fission yield n_f^{tot}	Total fission cross section [mb]
370	0.00359	86 ± 2	66 ± 2	3.6 ± 2	2.0 ± 1	2.1 ± 1.0	0.00629 ± 0.00031	123 ± 7
500	0.00630	88 ± 2	94 ± 2	3.8 ± 2	2.1 ± 1	1.7 ± 0.5	0.00762 ± 0.00031	149 ± 8
650	0.00716	87 ± 2	99 ± 1	4.0 ± 2	2.2 ± 1	1.1 ± 0.5	0.00838 ± 0.00030	164 ± 8

The present results are consistent with the measurements using proton-induced fission on ^{208}Pb between 50 and 200 MeV obtained by Flerov (diagonal crosses) [55], Shigaev (crosses) [56] and Duijvestijn (open star) [57]. The same occurs when one compares our data with the measurements of ^{nat}Pb between 50 and 200 MeV, which were performed by Shigaev (open triangles up) [56], Duijvestijn (open triangle down) [57], and Bychenkov (open squares) [58], as well as with the values reported by Konshin (stars) [59] between 150 and 400 MeV. Moreover, the results obtained by Enqvist and collaborators (open circle) [37] with ^{208}Pb at 1*A* GeV using the magnetic spectrometer FRS also seems consistent with the extrapolation of our data. One can observe that the cross section obtained by Gloris (open diamond) [60,61] with ^{nat}Pb at 1 GeV is consistent with the previous measurement of Enqvist and collaborators (open circle) because, as already mentioned, the measurements performed with ^{nat}Pb must be above those with ^{208}Pb.

Our measurements are also in agreement with the values reported by Hagebo (open cross) [62] and Brandt (full star) [63], who measured in direct kinematics the reaction $p + ^{nat}$Pb at 600 and 590 MeV, respectively. Finally, the results reported by Kotov (small full squares) [64] measuring proton-induced fission on ^{nat}Pb covering a large range of kinetic energies show a systematic underestimation of the cross sections compared to the other measurements. However, the relative evolution of Kotov's data with the proton energy confirms the tendency shown by our data between 300 and 700 MeV and the extrapolation up to 1 GeV. One can also observe that the measurement reported by Vaishnene (full triangle down) [65] at 1 GeV presents the same underestimation.

The new measurements together with the validated data for other energies were used to benchmark the parametrization of total fission cross sections for proton-induced reactions on ^{208}Pb performed by Prokofiev [40]. The parametrization shown in Eq. (1) was first proposed by Fukahori and Pearlstein [66] and later modified by Prokofiev to take into account the reduction of the fission cross sections at energies above 1 GeV:

$$\sigma_f(E) = P_1(1 - e^{-P_3(E-P_2)})[1 - P_4 \ln(E)]. \quad (1)$$

Figure 11 shows the measurements obtained in this work (full circles) together with the data reported by Schmidt (full triangle up) [39], Enqvist (open circle) [37], Flerov (open squares) [55], Shigaev (crosses) [56], and Duijvestijn (open star) [57] in comparison to the systematics proposed by Prokofiev [40] for ^{208}Pb(p, f) reactions (dashed line). Clearly the systematics of Prokofiev underestimates the data

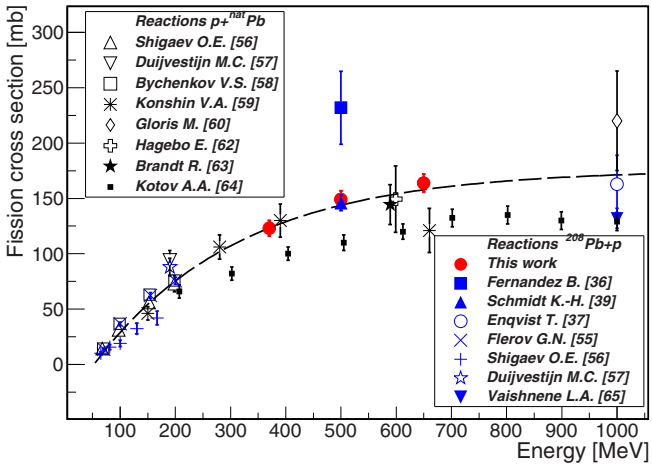

FIG. 10. (Color online) Total fission cross sections measured in the present work (full circles) as a function of the proton energy in comparison to previously measured data for the reactions $p + ^{nat}$Pb and ^{208}Pb + p. The dashed line is to guide the eye.

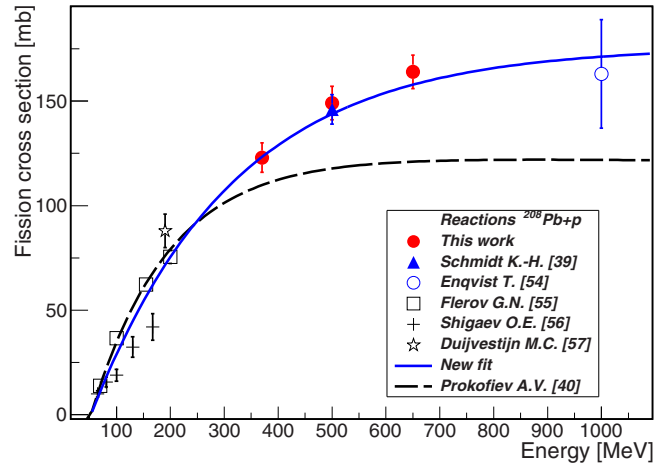

FIG. 11. (Color online) Comparison between Prokofiev's systematics for proton-induced fission on ^{208}Pb (dashed line) and different measurements (symbols). The full line represents a fit of the new data using Prokofiev's equation.

TABLE II. Parameters of the parametrization of the total fission cross sections for the reaction $p + ^{208}$Pb obtained in this work and the ones previously proposed by Prokofiev.

P_1	P_2	P_3	P_4	χ^2/ν	Reference
179	52.8	0.00378	0.00203	6.76	This work
142	52.7	0.00665	0.00203	1.26	Prokofiev [40]

for energies larger than 300 MeV while at low energies the systematic seems to reproduce the data fairly well. This is an expected result because the systematics were obtained by fitting the low-energy measurements and the one at 1 GeV reported by Vaishnene and collaborators [65]. However, we have only taken into account the measurement of Enqvist and collaborators [37] because it is in better agreement with the tendency of our data.

In order to obtain a better parametrization of the proton on lead total fission cross sections, we have repeated the fit using the data shown in Fig. 11. In this fit we fixed the parameter P_4 to the same value given by Prokofiev to avoid divergences because of the limited number of measurements above 700 MeV. The new values of the parameters are shown in Table II and are compared with the previous ones obtained by Prokofiev. The result of this new fit is also shown in Fig. 11 as the full line.

IV. DISSIPATIVE AND TRANSIENT EFFECTS

Different experimental observables such as the pre-scission particle emission [67,68] or the fission cross sections indicate that fission at excitation energies above 100 MeV cannot be explained by purely statistical approaches like the transition-state method [12]. However, a description according to a diffusion process across the fission barrier seems more appropriate [25,69]. In this picture, a dissipation coefficient couples the intrinsic and collective degrees of freedom determining how fast excitation energy is transformed into deformation. This coupling between excitation energy and deformation together with the stochastic nature of the process introduces an average time, or transient time, that the system needs to reach a stationary fission flux across the barrier. The natural framework to describe these processes are transport equations such as the Fokker–Planck [22,70] or Langevin [71–73] equations including the nuclear potential against deformation, a dissipative and a stochastic term.

Grangé and collaborators [22] established that the optimal conditions for investigating low-deformation dissipative and transient effects in fission were the use of spherical fissioning systems with low-angular momentum and excitation energies well above the fission barrier. Several works tried to fulfill these conditions at least partially. A first example is alpha-induced fusion-fission reactions on tungsten targets at energies up to 140 MeV [74]. This experiment demonstrated that the measured excitation functions for the fission cross sections were compatible with a value of the transient time less than $\tau_{\text{trans}} = 1 \times 10^{-21}$ s. Spallation reactions have also been used to induce fission in tantalum [75], gold [76], and uranium [77] targets. In these cases excitation energies up to several hundreds of MeV were reached and relatively low angular momentum was induced, but for the tantalum and uranium cases the fissioning systems were deformed. To describe the measured cross sections, calculations taking into account the initial deformation required dissipative and transient effects. The value of the reduced dissipation parameter used to describe the data was around $(4.5 \pm 0.5) \times 10^{21}$ s^{-1} and its corresponding transient time was $(3.3 \pm 0.7) \times 10^{-21}$ s. Similar results were obtained in peripheral fragmentation reactions induced by different pre-actinides on a carbon target [78].

For the reaction investigated in this work, fission induced by relativistic protons onto a lead target fulfills all the optimum requirements for the investigation of dissipative and transient effects in fission. Moreover, the combination of our measurements with validated previous measurements, as discussed in Sec. III, will help to provide a complete excitation function for the fission cross section of this reaction that will be used to investigate the onset of transient effects.

For the description of the data we have coupled two reaction codes. The Liège intranuclear cascade code INCL4.6 [53] describes the fast interaction between the proton and the lead target as a series of nucleon-nucleon collisions leading to an excited remnant. The deexcitation of this remnant is modeled by the statistical evaporation code ABLA07 [54]. In this code, dissipative and transient effects in fission are described by using an analytical description of the time-dependent fission width as obtained from a Fokker–Planck equation describing the diffusion across the barrier, as indicated in Ref. [79].

In Fig. 12 we show different calculations compared with the data obtained in this work and with other data validated in Sec. III. In this figure, the dashed line represents the result of a calculation taking dissipative effects with a value of the reduced dissipation parameter $\beta = 4.5 \times 10^{21}$ s^{-1} into account, but not considering transient effects. These

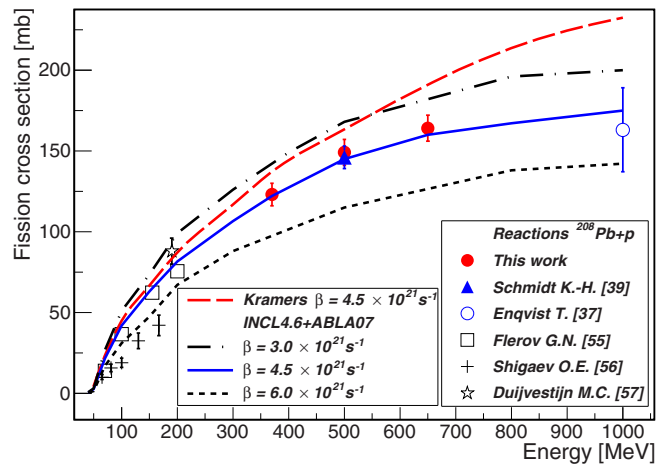

FIG. 12. (Color online) Fission cross sections measured in this work (full circles) and in other experiments in comparison with a the dynamical description of fission based on a time-independent fission width given by Kramers (long-dashed line) and with calculations using INCL4.6 + ABLA07 for different values of the reduced dissipation parameter.

calculations correspond to the description of the fission process proposed by Kramers [19]. As can be seen, this calculation clearly overestimate the fission cross sections at high proton energies. However, the calculations describe rather well the cross sections for proton energies below 200 MeV. This result is in agreement with other works [22,25,75], where the authors did not observe transient-time effects for excitation energies below 100–150 MeV.

In the same figure, the solid line corresponds to calculations considering a time-dependent fission width using the same value for the reduced dissipation parameter, $\beta = 4.5 \times 10^{21}$ s^{-1}, according to the prescription proposed in Ref. [79]. As can be seen, this calculation nicely describes the complete excitation function of fission cross sections. The comparison with the calculations without transient effects would indicate that these effects appear at excitation energies above 110 MeV. This onset of transient effects at relatively high excitation energies can be understood if one takes into account that the average fission delay induced by a reduced dissipation parameter $\beta = 4.5 \times 10^{21}$ s^{-1} corresponds to $\tau_{\text{trans}} = 1.2 \times 10^{-21}$ s. Therefore, such a short time shift can only be significant when the statistical time is of the same order.

The dotted-dashed and dotted lines in Fig. 12 represent similar calculations but with different values of the reduced dissipation parameter, $\beta = 3 \times 10^{21}$ s^{-1} and $\beta = 6 \times 10^{21}$ s^{-1}, respectively. These additional calculations were used to illustrate that all cross sections can be described with the same value of the reduced dissipation parameter and, consequently, no evidence for a temperature dependence is observed. These conclusions, the onset of transient effects at excitation energies above 110 MeV, and the temperature independence of the reduced dissipation parameter coincide with the ones obtained in other works [22,25,26,75].

In order to benchmark our data and validate the model calculations, in Fig. 13 we also analyze neutron-induced fission cross sections on natural lead over the same range of energy covered by our data, but investigated in direct kinematics. The open circles represent a rather complete set of data up to 200 MeV obtained by Shcherbakov and collaborators [81]. The open diamonds correspond to the only existing set of data for energies above 200 MeV measured by Tarrio and collaborators [80]. The cross sections above 200 MeV were measured relative to ^{235}U. Absolute values were obtained using evaluated total fission cross sections of ^{235}U taken from the JENDL/HE-2007 evaluation [82,83].

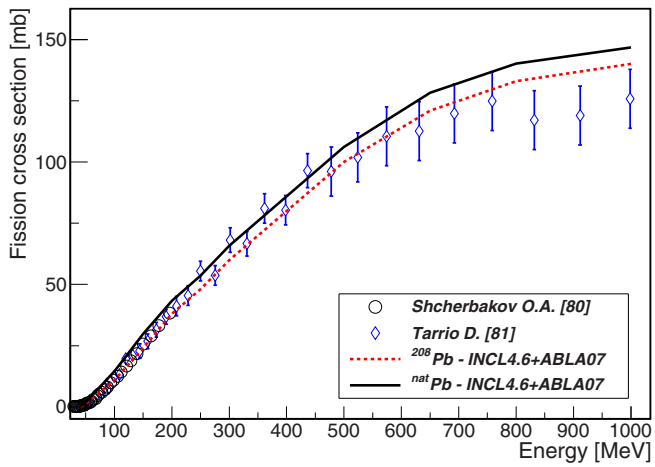

FIG. 13. (Color online) Fission cross sections measured for neutron-induced reactions on $^{\text{nat}}$Pb [80,81]. The solid and dotted lines represent calculations using INCL4.6 + ABLA07 with a reduced dissipation parameter of $\beta = 4.5 \times 10^{21}$ s^{-1} for fission reactions induced by neutrons on $^{\text{nat}}$Pb and ^{208}Pb, respectively.

In this figure we also include the same model calculations we performed for the proton data for a value of the reduced dissipation parameter $\beta = 4.5 \times 10^{21}$ s^{-1}. The dotted line corresponds to calculations for ^{208}Pb and the solid line for $^{\text{nat}}$Pb. Because the difference of the total fission cross section between the two targets is smaller than 10%, we can then directly compare the proton data with ^{208}Pb and neutron data with $^{\text{nat}}$Pb. The calculations shown in Fig. 13 reproduce the data very well up to 550 MeV and within the error bars up to 750 MeV. Above that energy, the calculations overestimate the data. Proton-induced fission reactions have been intensively investigated at GSI at energies around 1000A MeV with tantalum [75], gold [76], lead [37], and uranium targets [77]. Total fission cross sections obtained in these measurements were reasonably well reproduced by the same model calculations and parameters [53,75] we use to describe the neutron-induced fission cross sections shown in Fig. 13. This validation of our model calculations with reactions induced by protons around 1 GeV and the good description of the neutron data at energies below 750 MeV could indicate some problem with the data shown in Fig. 13 above 750 MeV, which would be also supported by the unexpected reduction in the measured cross sections above that energy value.

The overall good description of the neutron-induced fission cross sections with the same model calculations that also reproduce the proton-induced fission allows us to validate two independent sets of data, at least up to 650 MeV, and represents an additional support to the conclusions obtained with respect to the magnitude and temperature independence of the reduced dissipation parameter.

V. CONCLUSIONS

In the present work, we investigated proton-induced fission of ^{208} Pb in inverse kinematics at 370A, 500A, and 650A MeV by using a highly efficient detection setup that permitted us to determine the fission cross sections with high precision. These new data allow us to clarify the existing discrepancies in previous measurements at intermediate and high energies.

This set of data also helps us to revisit the previously established systematics by Prokofiev [40] and to propose a new parametrization for proton-induced fission cross sections. Moreover, we use the data to benchmark model calculations performed with the intranuclear cascade code, INCL4.6 [53], coupled to the deexcitation code ABLA07 [54]. The large range covered by these data in terms of excitation energy allows us to investigate dissipative and transient effects in fission. Calculations including dissipative but not transient effects

could describe the measured cross sections up to a proton energy of around 200 MeV. At higher excitation energies, only calculations including a time-dependent description of the fission width describe the data correctly. We then confirm previous works pointing to a unique value of the reduced dissipation parameter around $\beta = 4.5 \times 10^{21}$ s^{-1} as well as to the temperature independence of this parameter. In addition, we confirm that the onset of transient effects occurs at excitation energies around 110 MeV [22,25,26,75].

Finally, we also analyze neutron-induced fission cross sections on ^{nat}Pb investigated in direct kinematics and covering the same range in energy investigated with protons in this work. The fact that the same model calculations also describe the neutron-induced-fission cross sections, at least up to 650 MeV, reinforces our previous conclusions on the role of dissipative and transient effects in fission.

ACKNOWLEDGMENTS

The authors are indebted to the GSI accelerator staff for providing an intense and stable beam of ^{208}Pb. We also gratefully acknowledge J.-M. Gheller and S. Leray for providing the liquid hydrogen target and G. Ickert, D. Körper, N. Kurz, and A. Prochazka for their technical support during the experiment. This work was partially supported by the European Commission under projects ANDES-FP7-249671 and CHANDA-FP7-605203, the Spanish Ministry of Research and Innovation under projects FPA2010-22174-C02 and Consolider-CPAN-CSD2007-00042, and the Regional Government of Galicia under the program "Grupos de Referencia Competitiva 2013-011." One of us, C.R.T., also acknowledges the support of the Spanish Ministry of Education under a grant of postdoctoral mobility (2011) administered by FECYT.

[1] N. Schunck, J. Phys.: Conf. Ser. **436**, 012058 (2013).
[2] M. Bender *et al.*, Rev. Mod. Phys. **75**, 121 (2003).
[3] B. Jurado *et al.*, Phys. Lett. B **553**, 186 (2003).
[4] C. Paradela *et al.*, Phys. Rev. C **82**, 034601 (2010).
[5] Q. Ducase *et al.*, EPJ Web Conf. **62**, 08002 (2013).
[6] J. Benlliure, E. Casarejos, J. Pereira, and K. H. Schmidt, Phys. Rev. C **74**, 014609 (2006).
[7] A. Bail *et al.*, Phys. Rev. C **84**, 034605 (2011).
[8] J. Benlliure *et al.*, Nucl. Phys. A **628**, 458 (1998).
[9] F. Farget *et al.*, J. Phys.: Conf. Ser. **420**, 012119 (2013).
[10] K. Nishio *et al.*, Phys. Rev. C **82**, 024611 (2010).
[11] A. Boudard *et al.*, Nucl. Phys. A **740**, 195 (2004).
[12] N. Bohr and J. A. Wheeler, Phys. Rev. **56**, 426 (1939).
[13] E. Holub, D. Hilscher, G. Ingold, U. Jahnke, H. Orf, and H. Rossner, Phys. Rev. C **28**, 252 (1983).
[14] W. P. Zank, D. Hilscher, G. Ingold, U. Jahnke, M. Lehmann, and H. Rossner, Phys. Rev. C **33**, 519 (1986).
[15] T. Geisel and J. Nierwetberg, Phys. Rev. Lett. **48**, 835 (1982).
[16] A. Gavron *et al.*, Phys. Lett. B **176**, 312 (1986).
[17] A. Gavron *et al.*, Phys. Rev. C **35**, 579 (1987).
[18] D. J. Hinde *et al.*, Nucl. Phys. A **452**, 550 (1986).
[19] H. A. Kramers, Physica **7**, 284 (1940).
[20] P. Grangé and H. A. Weidenmüller, Phys. Lett. B **96**, 26 (1980).
[21] K. H. Bhatt, P. Grangé, and B. Hiller, Phys. Rev. C **33**, 954 (1986).
[22] P. Grangé, Li Jun-Qing, and H. A. Weidenmüller, Phys. Rev. C **27**, 2063 (1983).
[23] P. Fröbrich, I. I. Gonchar, and N. D. Mavlitov, Nucl. Phys. A **556**, 281 (1993).
[24] I. I. Gonchar, Phys. Part. Nucl. **26**, 294 (1995).
[25] J. P. Lestone and S. G. McCalla, Phys. Rev. C **79**, 044611 (2009).
[26] C. Schmitt, K.-H. Schmidt, A. Kelic, A. Heinz, B. Jurado, and P. N. Nadtochy, Phys. Rev. C **81**, 064602 (2010).
[27] Spallation Neutron Source at OAK Ridge National Laboratory http://www.sns.gov/
[28] J-PARC, Japan Proton Accelerator Research Complex http://j-parc.jp/index-e.html
[29] China Spallation Neutron Source (CSNS) http://csns.ihep.ac.cn/english/index.htm
[30] European Spallation Source http://europeanspallationsource.se/
[31] J. L. Biarrotte *et al.*, Nucl. Instrum. Methods Phys. Res. Sect. A **562**, 656 (2006).
[32] H. Aït Abderrahim *et al.*, Nucl. Instrum. Methods Phys. Res. Sect. A **463**, 487 (2001).
[33] C. D. Bowman, Annu. Rev. Nucl. Part. Sci. **48**, 505 (1998).
[34] M. Medarde *et al.*, J. Nucl. Mater. **411**, 72 (2011).
[35] A. J. Koning, J.-P. Delaroche, and O. Bersillon, Nucl. Instrum. Methods Phys. Res., Sect. A **414**, 49 (1998).
[36] B. Fernández-Domínguez *et al.*, Nucl. Phys. A **747**, 227 (2005).
[37] T. Enqvist *et al.*, Nucl. Phys. A. **686**, 481 (2001).
[38] J. Benlliure *et al.*, Nucl. Instrum. Methods Phys. Res. A **478**, 493 (2002).
[39] K.-H. Schmidt *et al.*, Phys. Rev. C **87**, 034601 (2013).
[40] A. V. Prokofiev, Nucl. Instrum. Methods Phys. Res., Sect. A **463**, 557 (2001).
[41] A. Bail, J. Taieb, A. Chatillon, G. Belier, B. Laurent, and E. Pellereau, *Proceedings of the 2nd International Conference on Advancements in Nuclear Instrumentation Measurement Methods and their Applications* (ANIMMA-IEEE, Ghent, Belgium, 2011).
[42] E. Pellereau *et al.*, EPJ Web Conf. **62**, 06005 (2013).
[43] G. Boutoux *et al.*, Phys. Procedia **47**, 166 (2013).
[44] J. L. Rodríguez-Sánchez *et al.*, EPJ Web Conf. **62**, 07009 (2013).
[45] A. Ebran *et al.*, Nucl. Instrum. Methods Phys. Res., Sect. A **728**, 40 (2013).
[46] M. Pfüzner *et al.*, Nucl. Instrum. Methods Phys. Res., Sect. B **86**, 213 (1994).
[47] R. Janik *et al.*, Nucl. Instrum. Methods Phys. Res., Sect. A **640**, 54 (2011).
[48] P. Chesny *et al.*, GSI Annu, Rep. **97**, 190 (1996).
[49] B. Voss, *Proceedings of the Nuclear Science Symposium and Medical Imaging Conference* (NSS/MIC-IEEE, Valencia, Spain, 2011).
[50] C. Finck *et al.*, J. Phys.: Conf. Ser. **50**, 397 (2006).
[51] http://geant4.cern.ch/
[52] D. Bertini, J. Phys.: Conf. Ser. **331**, 032036 (2011).
[53] A. Boudard, J. Cugnon, J. C. David, S. Leray, and D. Mancusi, Phys. Rev. C **87**, 014606 (2013).
[54] A. Kelić, M. V. Ricciardi, and K.-H. Schmidt, *Proceedings of Joint ICTP-IAEA Advanced Workshop on Model Codes for Spallation Reactions, ICTP Trieste, Italy, 2008*, edited by

D. Filges, S. Leray, Y. Yariv, A. Mengoni, A. Stanculescu, and G. Mank (IAEA INDC(NDS)-530, Vienna, 2008), pp. 181–221.
[55] G. N. Flerov *et al.*, S. J. At. Energy **33**, 1144 (1972).
[56] O. E. Shigaev *et al.*, Khlopin Radiev. Inst., Leningrad Reports, No. 17, 1973.
[57] M. C. Duijvestijn, A. J. Koning, J. P.M. Beijers, A. Ferrari, M. Gastal, J. vanKlinken, and R. W. Ostendorf, Phys. Rev. C **59**, 776 (1999).
[58] V. S. Bychenkov *et al.*, Sov. J. Nucl. Phys. **17**, 496 (1973).
[59] V. A. Konshin *et al.*, Yad. Fiz. **2**, 682 (1965).
[60] M. Gloris, *et al.*, Nucl. Instrum. Methods Phys. Res., Sect. A **463**, 593 (2001).
[61] R. Michel, *et al.*, Nucl. Instrum. Methods Phys. Res., Sect. B **129**, 153 (1997).
[62] E. Hagebø and T. Lund, J. Inorg. Nucl. Chem. **37**, 1569 (1975).
[63] R. Brandt *et al.*, Rev. Phys. Appl. **7**, 243 (1972).
[64] A. A. Kotov *et al.*, Phys. Rev. C **74**, 034605 (2006).
[65] L. A. Vaishnene *et al.*, Z. Phys. A **302**, 143 (1981).
[66] T. Fukahori and S. Pearlstein, IAEA Report INDC(NDS) **245**, 93 (1991).
[67] D. Hilsher and H. Rossner, Ann. Phys. (Paris) **17**, 471 (1992).
[68] J. P. Lestone, Phys. Rev. C **59**, 1540 (1999).
[69] B. Jurado *et al.*, Phys. Rev. Lett. **93**, 072501 (2004).
[70] S. Chandrasekhar, Rev. Mod. Phys. **15**, 1 (1943).
[71] Y. Abe *et al.*, Phys. Rep. **275**, 49 (1996).
[72] P. Fröbrich and I. I. Gontchar, Nucl. Phys. A **563**, 326 (1993).
[73] P. N. Nadtochy, G. D. Adeev, and A. V. Karpov, Phys. Rev. C **65**, 064615 (2002).
[74] K. X. Jing *et al.*, Phys. Lett. B **518**, 221 (2001).
[75] Y. Ayyad *et al.*, Phys. Rev. C **89**, 054610 (2014).
[76] J. Benlliure *et al.*, Nucl. Phys. A **700**, 469 (2002).
[77] M. V. Ricciardi *et al.*, Phys. Rev. C **73**, 014607 (2006).
[78] B. Jurado *et al.*, Nucl. Phys. A **757**, 329 (2005).
[79] B. Jurado *et al.*, Nucl. Phys. A **747**, 14 (2005).
[80] D. Tarrio *et al.*, Phys. Rev. C **83**, 044620 (2011).
[81] O. A. Shcherbakov *et al.*, J. Nucl. Sci. Technol. Suppl. **2**, 230 (2002).
[82] T. Fukahori *et al.*, J. Nucl. Sci. Technol. Suppl. **2**, 25 (2002).
[83] Y. Watanabe *et al.*, J. Korean Phys. Soc. **59**, 1040 (2011).